Spatially and temporally resolved IR-DFWM measurement of HCN released from gasification of biomass pellets

Hot, Dina; Pedersen, Rasmus L.; Weng, Wubin; Zhang, Yuhe; Aldén, Marcus; Li, Zhongshan

Published in:
Proceedings of the Combustion Institute

DOI:
10.1016/j.proci.2018.07.105

2019

Document Version:
Publisher's PDF, also known as Version of record

Available online at www.sciencedirect.com

ScienceDirect

Proceedings of the Combustion Institute 37 (2019) 1337–1344

Proceedings of the Combustion Institute

www.elsevier.com/locate/proci

Spatially and temporally resolved IR-DFWM measurement of HCN released from gasification of biomass pellets

Dina Hot, Rasmus L. Pedersen, Wubin Weng, Yuhe Zhang, Marcus Aldén, Zhongshan Li*

Division of Combustion Physics, Department of Physics, Lund University, P.O. Box 118, SE-221 00 Lund, Sweden

Received 30 November 2017; accepted 20 July 2018
Available online 8 August 2018

Abstract

For the first time, to the best of the authors' knowledge, nonintrusive quantitative measurement of hydrogen cyanide (HCN) released during the devolatilization phase of straw pellets gasification is demonstrated with high spatial and temporal resolution. Mid-infrared degenerate four-wave mixing (IR-DFWM) measurements of HCN were performed by probing the interference-free P(20) line in the ν_1 vibrational band at around 3 μm and the IR-DFWM signal was detected with an upconversion-based detector, providing discrimination of thermal noise and increased sensitivity. A novel single-pellet setup consisting of a multi-jet burner was used to provide hot flue gas environments with an even and well-defined temperature distribution, for single straw pellet gasification at atmospheric pressure. The environments had temperatures of 1380 K, 1540 K and 1630 K with a constant oxygen concentration of 0.5 vol%. In order to quantify the amount of HCN released during the devolatilization of straw pellets, calibration measurements were performed in well-defined HCN gas flows. Selected hot water lines were probed with IR-DFWM in the interrogated volume to obtain the instantaneous temperature, which were used to correct the temperature effect. HCN concentrations up to 1500 ppm were detected during the devolatilization stage, and the results indicate a strong temperature dependence of the HCN release.

Keywords: Degenerate four-wave mixing; Upconversion detection; Mid-infrared; Biomass; HCN concentration

1. Introduction

Biomass is an important renewable energy source, which is aimed for replacing part of the fossil fuels with its sustainable supply and CO_2 neutrality. Some biomass fuels, such as agricultural residue, can have high nitrogen content, which can be transferred to NO_x during combustion [1,2]. With the increasingly strict environmental standard, more research on the nitrogen conversion behavior is needed to reduce the NO_x emission. Large amounts of the fuel-nitrogen in biomass

* Corresponding author.
E-mail address: zhongshan.li@forbrf.lth.se (Z. Li).

https://doi.org/10.1016/j.proci.2018.07.105

can be released during the devolatilization stage of combustion/gasification as ammonia (NH_3), hydrogen cyanide (HCN) or isocyanic acid (HNCO) [1–4]. When the environment temperature is above 850–900 K, the release fraction in this stage can be about 80% [2], which corresponds to about 70% volatile matter in most biomass [5]. NH_3, HCN and HNCO are important precursors of NO_x, and the investigation of their production rate and fraction is essential in the nitrogen chemistry study, which are affected by heating rate, particle size, atmosphere and mineral matters [1,3]. Numerous research works exist related to measurements of released volatile-N mainly through FT-IR and chemical absorption techniques where significant discrepancies between them were found. It was considered to be due to the use of sampling methods since secondary reactions may take place before the gas analysis, such as HNCO may be hydrolyzed to NH_3 when using chemical absorption technique [1,2]. Sampling-based techniques were also proved to be inapplicable for detection of NH_3 and HCN due to their high hygroscopicity and reactivity.

Laser-based diagnostic techniques are widely used in combustion research since they provide non-intrusive, *in situ* measurement with the possibility of high spatial and temporal resolution. As the HCN molecule lacks electronic transitions in the UV/visible spectral regions, but is infrared active and has accessible vibrational bands in the infrared spectral region, its detection has been performed in the near or mid-infrared by probing absorption lines in the fundamental vibrational band, v_1, around 3.04 μm or the overtone vibrational bands, v_2 and v_3, around 1.54 μm and 1.04 μm, respectively [6,7]. Previous detection of HCN in flames has been performed using absorption techniques such as wavelength modulation absorption spectroscopy (WMAS) by probing absorption lines in v_2 [8] as well as continuous-wave cavity ring-down spectroscopy by probing HCN rotational lines in the v_2 and v_3 vibrational bands, respectively [9,10]. However, even though these techniques provide high sensitivity, its application for *in situ* measurement in flame environments were hindered by the strong interference from hot water lines and the line-of-sight nature of the techniques.

Non-linear laser techniques based on wave-mixing provide coherent signal with high spatial resolution, sensitivity and discrimination against the background scattering, which are favorable in the harsh environment during biomass combustion/gasification. Kiefer and Ewart [11] reviewed the non-linear techniques that are applied for minor species detection in combustion research. Sensitive detection of infrared-active molecules by probing the strong fundamental stretching bands using mid-infrared polarization spectroscopy (IRPS) has been successfully demonstrated for some combustion important molecules, i.e. CH_4 [12], C_2H_6 [13], C_2H_2 [14,15], OH [16], CO_2 and H_2O [17]. Sun et al. [18] showed the possibility of *in situ* measurement of HCN in laminar flames using IRPS. High quality polarizers are of utmost important to polarization spectroscopy and the extinction ratio of the available polarizers in the mid-infrared sets the detection limit of IRPS technique. Degenerate four-wave mixing (DFWM) is another non-linear technique and was firstly presented by Abrams and Lind [19,20] and is nowadays a mature non-linear technique. Mid-infrared degenerate four-wave mixing (IR-DFWM) has been applied for sensitive CH_4 and C_2H_2 detection [21]. The complexity involved accurate alignment of three invisible beams and the precise location of the signal beam has hindered practical applications of this sensitive and background-free IR-DFWM technique.

Sun et al. [22] designed a set of BOXCARS plates to facilitate a stable forward phase-matching alignment of the IR-DFWM setup and this approach was demonstrated for HCl and acetylene detection. Besides the detection of minor species, the IR-DFWM was also demonstrated for temperature measurement [23] by using the temperature sensitive water lines in the spectral interval 3230–3232 cm^{-1}. The main difficulty of working in the mid-IR is the cryogenically cooled InSb detectors, which have high thermal noise. Recently, a low noise upconversion-based detector has been demonstrated [24] together with IR-DFWM [25] and IRPS [26] for detection of acetylene and methane, respectively.

In this work, we demonstrate quantitative *in situ* IR-DFWM measurements of HCN released during gasification of straw pellets at three different gasification environment temperatures, i.e. 1380 K, 1540 K and 1630 K, at atmospheric pressure. The HCN detection was performed during the devolatilization stage of the biomass gasification by centering the laser on the P(20) absorption line in the fundamental vibrational band v_1. The released HCN concentration was retrieved after calibration measurement of known HCN concentration and with full consideration of the temperature dependence of the HCN signal. An upconversion-based detector was used to improve the sensitivity.

2. Experimental setup

2.1. IR-DFWM and upconversion detector

A schematic view of the experimental setup is shown in Fig. 1. The laser system providing mid-IR laser radiation has previously been described in more detail [17] and hence only a brief description is given here. Laser radiation of 3 μm was generated by a laser system consisting of an injection-seeded Nd:YAG laser (Spectra Physics, PRO 290-10), a dye laser (Sirah, PRSC-D-18) and a

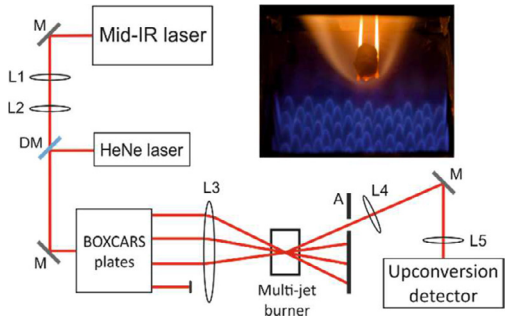

Fig. 1. Schematic view of the IR-DFWM setup. M: gold mirror, DM: dichroic mirror, L1: CaF_2 lens, $f = 500$ mm, L2: CaF_2 lens, $f = -200$ mm, L3: CaF_2 lens, $f = 500$ mm, L4: CaF_2 lens, $f = 500$ mm, L5: CaF_2 lens, $f = 100$ mm, A: aperture. The photograph shows an angled top view of the multi-jet burner with gasification of a straw pellet.

difference frequency mixing unit. The fundamental output of the Nd:YAG laser (1064 nm) was frequency doubled to 532 nm to pump the tunable dye laser (LDS798). The dye laser output tuned to 790 nm was difference frequency mixed with a part of the residual 1064 nm beam from the Nd:YAG laser in a $LiNbO_3$ crystal, resulting in IR laser pulses. This IR laser beam was amplified in a second $LiNbO_3$ crystal pumped with another part of the residual 1064 nm beam, producing pulsed tunable mid-IR laser radiation with pulse energy of 4 mJ and pulse duration of 3–4 ns. In the work by Li et al. [17], the linewidth of the IR laser has been measured to be 0.025 cm^{-1}.

The infrared laser beam was guided through a telescope arrangement (L1, L2) to obtain a beam size of 2 mm and was spatially overlapped with a HeNe laser beam through a dichroic mirror (DM) to facilitate the optical alignment. The IR beam was split into four parallel beams using a set of specially coated BOXCARS plates [22]. Three of these beams were focused by an $f = 500$ mm CaF_2 lens (L3) into a crossing point 3 mm above the burning pellets and the signal was generated along the pathway of the fourth beam. The probe volume was estimated to be $0.4 \times 0.4 \times 6$ mm^3. The IR-DFWM was collimated by another $f = 500$ mm CaF_2 lens (L4) and focused (L5) onto the upconversion detector. The IR signal is upconverted to shorter wavelengths in the detector using sum frequency generation with a 1064 nm mixing laser in a periodically poled lithium niobate crystal. The power of the mixing laser was 90–100 W. The poling period used was 21.5 μm, and the crystal was heated to 104.5 °C and 123 °C to phase match the HCN line and the water lines, respectively. The upconverted signal was near 790 nm in wavelength, and was detected using a time-gated silicon based camera (IDS model UI-3240CP-NIR-GL). The detector was triggered by the Nd:YAG laser with a time/delay generator (SRS, DG535).

2.2. Multi-jet burner and straw pellet

The straw pellets used in this study were cylindrically shaped with a diameter and length of 6 and 10 mm, respectively, and with a weight of 420 ± 40 mg. Characteristics of the straw pellets are presented in Table 1. The pellets were held by two ceramic rods (diameter 1 mm) and were placed in the hot gaseous environment provided by a laminar flame burner [27] consisting of 181 jets supporting premixed $CH_4/H_2/O_2/N_2$ flames with equivalence ratio around 0.95 and a N_2 co-flow evenly surrounding the jets. Details about the premixed flame conditions are summarized in Table 2. The flue gas temperatures were calibrated by two-line atomic fluorescence (TLAF) thermometry [27,28] and set to 1380 K, 1540 K or 1630 K with a constant oxygen content of 0.5 vol%. The photograph in Fig. 1 shows an angled top view of the multi-jet burner where the jet flames are visible together with gasification of a straw pellet. The IR-DFWM probe volume was located 3 mm right above the straw pellets. The burner was installed on a rail to enable a prompt moving in and out of the flame, which facilitated the optical alignment and definition of the starting time of each gasification/combustion operation.

2.3. Calibration measurement

In order to obtain quantitative HCN measurements, on-line calibrations were performed where concentration and temperature dependence of the HCN IR-DFWM signal recorded on the P(20) line (3248.48 cm^{-1}) was investigated in gas flows containing known admixtures of HCN diluted in nitrogen. The gas mixture flowed through an open T-shaped heating gas tube, made of fused silica surrounded by an electrical heating wire and insulation. A thermocouple (type K, ETI Ltd) was inserted through the top of the heating tube and the gas temperature was assumed to be uniform in the IR-DFWM crossing point. The IR-DFWM signal was recorded for temperatures between 296 K and 843 K, which is the operational temperature range of the heating tube. Temperature measurements using a thermocouple in this low temperature non-reactive flow are viable. The accurate *in situ* temperature values where HCN was practically measured are crucial for obtaining quantitative concentrations. However, thermocouple measurements are not adequate in these hot reactive flows. IR-DFWM probing the naturally available hot water lines was adopted in the work. The transient temperature values during the devolatilization stage of the straw pellets were recorded 3 mm above the pellet in the volatile plume for all flue gas temperatures and was obtained using the

Table 1
Characteristics of the straw pellets.

Low heating value (MJ/kg)	Proximate analysis (wt%, as received)				Ultimate analysis (wt%, dry ash free)				
	Volatiles	Fixed carbon	Moisture	Ash	Carbon	Hydrogen	Nitrogen	Sulfur	Oxygen
13.8	64.9	11.5	8.9	14.7	51.6	6.8	0.6	<0.01	41.0

Ash analysis (wt%, dry basis)

Na_2O	MgO	Al_2O_3	SiO_2	P_2O_5	SO_3	Cl	K_2O	CaO	Fe_2O_3	TiO_2	Other oxides
0.8	3.7	7.7	34.3	3.4	2.6	3.5	15.1	24.1	2.9	0.4	2.9

Table 2
Conditions for the premixed flame.

Case	Jet-flow(L/min)				Co-flow (L/min)	O_2 in flue gas (%)	Temperature of flue gas (K)
	CH_4	H_2	Air	N_2	N_2		
T1	2.53	0.44	26.07	2.20	7.70	0.5	1630
T2	1.98	0.88	21.82	2.20	9.90	0.5	1540
T3	0.88	3.52	17.70	7.70	11.00	0.5	1380

ratio between two temperature sensitive water line groups located at 3230–3232 cm^{-1}, which has previously shown to be sensitive for determining flame temperatures [23]. Description about the calibration process is found below.

3. Results and discussion

3.1. HCN concentration calibration

In order to convert the IR-DFWM signal to HCN concentration, a calibration measurement with known concentration is required where the optical setup is kept the same. In addition, a model is needed which includes the signal dependence on concentration and temperature. Our previous mid-IR DFWM works [22,23] using a similar laser system indicate that IR pulse energies above 1.5 mJ are needed to obtain a saturated excitation, while the IR pulse energy of 4 mJ is adopted in the present work to ensure a saturation condition. We base our approach on the work by Farrow et al. [29] with the assumption that the interaction length and laser intensity are constant for both calibration and real measurements. The DFWM signal is then described accordingly

$$I_{DFWM}(T, c) = a \cdot s(T) \cdot c^2 + b \quad (1)$$

where a is an experimentally determined constant, $s(T)$ is a scaling factor taking into account the temperature dependence of the line strength, the number density and the spectral overlap with the laser and c is the concentration. The offset, b, is the background mainly from light scattered or reflected at the surfaces of optics.

The scaling factor $s(T)$ is obtained by calculating the theoretical DFWM spectral line as a function of temperature

$$s(T) = \int_{w_l}^{w_h} (\sigma(T, w)N(T))^2 L(w, w_0)dw \quad (2)$$

where σ is the cross section calculated using the HCN data [30] presented in HITRAN2016 [7], N is the population calculated using the ideal gas law, and L is an estimate of the laser line shape centered at the line used for detection, w_0, which in this case is the HCN P(20) line in the ν_1 vibrational band. The lower and upper bound of the integral w_l and w_h, are in this case 3248 cm^{-1} and 3249 cm^{-1}, respectively. The calculation was validated by recording the IR-DFWM peak signal intensity of the HCN P(20) line at a constant HCN concentration of 300 ppm diluted in N_2 at temperatures between 296 K and 843 K. Collisional air-broadening which is provided in HITRAN is included in the simulation. The IR-DFWM signal is compared to the predicted scaling in Fig. 2. The measurements shown here were obtained by replacing the multi-jet burner shown in Fig. 1 with the electrical heating tube, and running a gas flow of 300 ppm HCN in N_2 through the heating tube. The temperature of the gas was determined using a thermocouple placed near the crossing point. At each measurement point the detected signal was taken when the gas temperature reached a stable value. The inset of Fig. 2 shows the simulated IR-DFWM signal of the P(20) line for temperatures 300 K and 1000 K, indicating intensity decrease at higher temperatures.

The constant a is determined by recording the IR-DFWM signal generated by a range of HCN concentrations in a gas flow diluted in N_2, and where a and b in Eq. (1) were fitted to the measured signal. This was done in the same setup described for the validating of the temperature dependence, but here the gas was kept at room temperature,

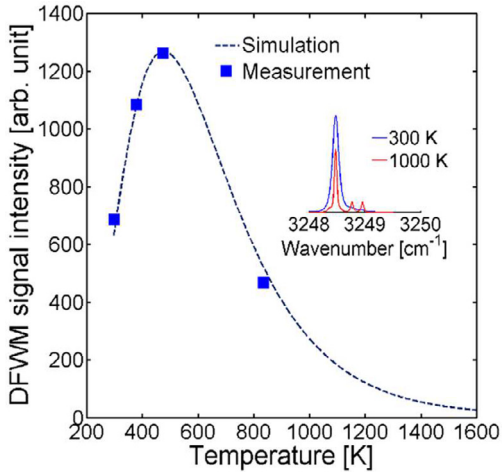

Fig. 2. The temperature dependence of the measured IR-DFWM peak signal for the HCN P(20) line at 300 ppm HCN concentration. Each measured point is an average of the peak value of 3 scans. The simulation is based on the data from HITRAN2016 for the P(20) line. Inset: Simulated IR-DFWM signal of HCN P(20) line for temperatures 300 K and 1000 K.

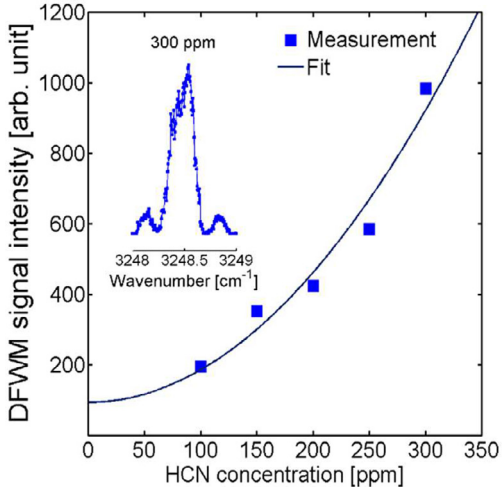

Fig. 3. IR-DFWM peak signal dependence on the HCN concentration diluted in N_2 at 296 K for the P(20) line from the v_1 band at 3248.48 cm^{-1}. Each point is an average of the peak value of 3 scans. The function fitted to the measurement data is given in Eq. (1). Inset: Scan of the P(20) line at 300 ppm HCN concentration.

296 K. The result is shown in Fig. 3, where the HCN concentration dependence of the IR-DFWM signal recorded on-peak of the P(20) line is shown. Each data point is an average of the peak value of 3 scans. A scan of the P(20) line for a HCN concentration of 300 ppm is shown in the inset, where the DC offset is due to the scattering background and

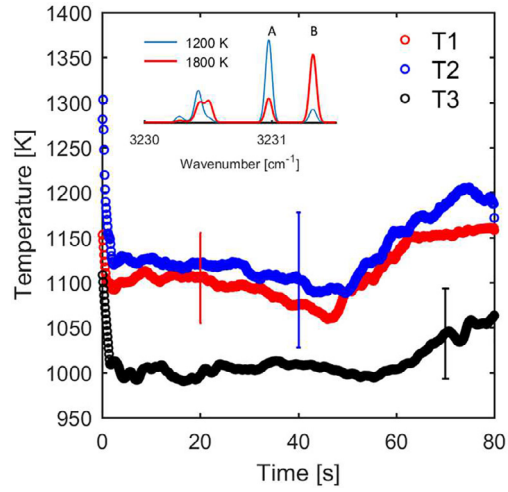

Fig. 4. Temperature measured 3 mm above the straw pellet during the devolatilization stage at the three different gasification conditions 1380 K (T3), 1540 K (T2) and 1630 K (T1). Inset: Simulated IR-DFWM scan of the temperature sensitive water line groups at 3230–3231.5 cm^{-1}. The temperature was retrieved according to the method presented in [23] where the on-line ratio between water line groups A and B was taken during the whole devolatilization stage. Ten on-line measurements were taken for each water line group and the graphs are an average of the 10 temperature measurements. The error bars indicate the average standard error, which is obtained to be ± 50 K for cases T1 and T3, and ± 75 K for case T2.

the minor side peaks and slightly asymmetric main peak can quite likely be attributed to some hiding etalon effects in the beam path. The detection limit at room temperature was found to be 100 ppm.

As the signal intensity is temperature dependent, the temperature of the measurement point must be determined, which was done using the method described by Sun et al. [23]. In that work, two groups of hot water lines were used due to the temperature dependence of their ratio which makes them useful for measuring temperature. The two groups of water lines are located near 3231 cm^{-1} and a simulated IR-DFWM spectrum showing the two water line groups is presented in the inset of Fig. 4 for two temperatures, 1200 K and 1800 K, where the groups are indicated as A and B, respectively. Sun et al. made a scan across the two hot water line groups and used the ratio of the line-integrated signal of the two groups to determine temperature. Scanning over the lines is possible for a time-independent signal. However, since the signal during the devolatilization stage of the straw pellet will vary with time, the temperature might change between scanning across the first group and the second. Instead the laser wavelength was kept constant at the peak of each of the two water line groups and the IR-DFWM water signal from 10

consecutive pellet measurements was recorded and averaged for each group. The ratio was then obtained for the averaged IR-DFWM water signals to determine the temperature in the measurement volume. Figure 4 shows the obtained temperature measured 3 mm above the burning straw pellet during the devolatilization stage. The measurements were performed for the three investigated gasification environment temperatures, 1380 K, 1540 K and 1630 K, referred as T3, T2 and T1, respectively. While the temperature above the pellet is expected to increase with increasing flue gas temperature, this is not the case for the values found for cases T1 and T2, which is probably due to the uncertainty in the determination of the temperature.

The determination of temperature is the main source of uncertainty in the calibration. The error bars shown in Fig. 4 are derived from the standard error of mean of 10 recordings. This is ± 50 K for cases T1 and T3, and ± 75 K in the case of T2. It takes into account variations of the laser pulse energy and the natural variation of pellet composition. This temperature method relies on the accuracy of tuning the laser to the center of the peak of each water line group, and inaccuracies in the spectral position of the laser line might give rise to systematic errors that are not taken into account here. Further investigation of the robustness of this method is needed.

From Eq. (1), the IR-DFWM signal intensity is now converted to concentration by

$$c = \left[\frac{I_{DFWM} - b}{as(T)}\right]^{1/2} \tag{3}$$

where a is the value retrieved from the concentration dependence, b is determined individually for each measurement, as the background level changes depending on the exact alignment and placement of the beam block shown in Fig. 1.

3.2. HCN release from straw pellets

The HCN release during the devolatilization stage of straw pellet gasification was investigated with IR-DFWM by using the calibration process described in the previous section. A typical HCN release history recorded on the P(20) line is presented in Fig. 5 for the gas environment temperature 1540 K (T2). Both the HCN release from a single pellet measurement as well as an average of 15 independent measurements are presented. The inset shows an excitation scan over the P(20) line recorded during the devolatilization stage. Due to the natural variation of the pellet composition, an initial study of the number of pellets required to get a representable average signal was performed. In total 30 independent measurements of the IR-DFWM HCN signal were recorded and the cumulative sum indicates that 10–15 pellets are sufficient to give an acceptable uncertainty on the measurement average. It is worth to note that the present

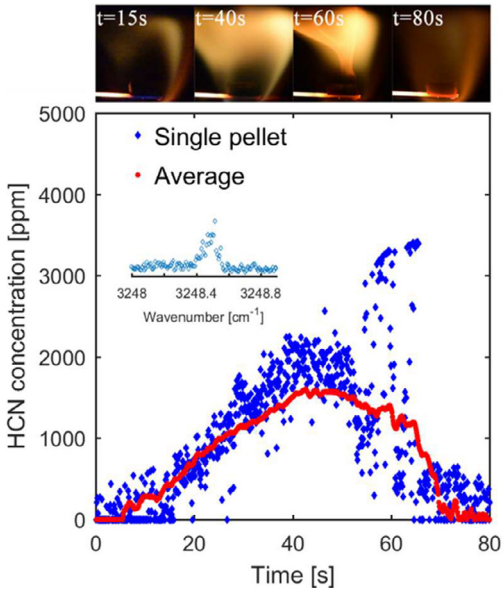

Fig. 5. Recorded HCN release during the devolatilization stage from gasification of a single straw pellet at the gasification environment temperature 1540 K (T2). The graph is an average of 15 independent recordings. The recording was performed on the P(20) line of HCN. Inset: Scan of the HCN P(20) line during the devolatilization stage. The photographs show the different stages of the measurement period.

IR-DFWM setup has a probe volume of 6 mm along the beam which is shorter than the volatile plume as shown in Fig. 5.

HCN was released as the pellet was loaded into the hot flue gas environment. The preheating period finished within the first ∼15 s, in which the HCN release intensity is quite weak corresponding to the weak volatile flame in the photograph at 15 s in Fig. 5. The release of HCN increased significantly after ∼15 s, and reached its peak at around 2000 ppm at roughly 40 s, when a sooty volatile flame was formed. After that, the HCN release declined gradually and was close to the value below the detection limit as no volatile gas was released from the pellet, indicating the start of the char gasification stage, which can be seen in the flame photograph at 80 s of Fig. 5. The main chemiluminescence originates from the excited sodium atoms released from the char. The whole HCN release duration is about 80 s, corresponding to the whole devolatilization stage. At 60 s, close to the end of the devolatilization stage, strong interference occurred due to the scattering signal from numerous large particles released from the pellet, which can be observed clearly in the middle of the sooty flame in the photograph at 60 s in Fig. 5. The occurrence of this visible particle stream directly from the straw pellet was always accompanied with the

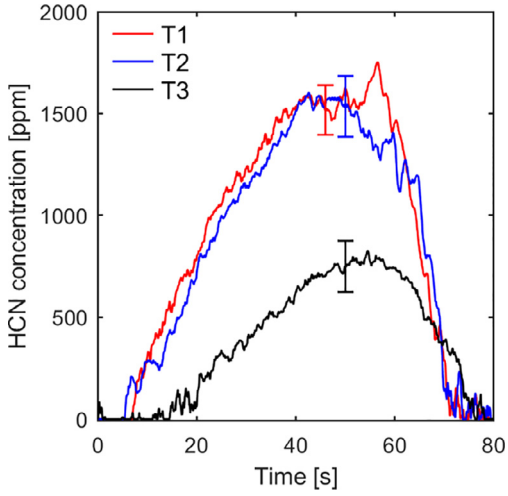

Fig. 6. Recorded HCN release during the devolatilization stage from gasification of straw pellets. Each graph is an average of 15 independent measurements of the HCN release recorded on the P(20) line for the three different gasification environments, 1380 K (T3), 1540 K (T2) and 1630 K (T1). The error bars indicate the average standard error in HCN concentration, which is obtained to be ± 10% throughout the whole HCN release.

strong scattering as shown in Fig. 5 at 60 s. The visible particle stream was observed to increase with the flue gas temperature, where no stream was observed for the temperature at case T3 whilst it was repeatedly present for the other two temperature cases. Measurements with flue gas temperatures higher than case T1 are difficult to perform due to the prevalent of the strong scattering stream. However, soot particles as shown in Fig. 5 at 40 s did not introduce extra background scattering from the mid-IR excitation laser beam as compared to the condition without the straw pellets. The occurrence of the particle stream coincides with the temperature increase of the volatile plume of the cases T1 and T2 as seen in Fig. 4. A possible explanation could be that the temperature of the pellets has a large increase at the end of the devolatilization stage, which could cause rapid decomposition of the char and break-off of large particles. This could be clarified with sampling techniques on large particles to determine the composition.

Figure 6 shows the averaged HCN release of 15 independent pellet measurements for each gasification environment temperature, 1380 K (T3), 1540 K (T2) and 1630 K (T1) recorded with the laser wavelength fixed on the peak of the P(20) line. The error bars represent the standard error of the mean concentrations of the released HCN, which is obtained to be ± 10% throughout the whole HCN release. For all temperature cases the trend of the HCN release seems to be similar, as described above with Fig. 5, but the release intensity is different. The temperature significantly enhanced the released HCN concentration as the ambient gas temperature increased from 1380 K (T3) to 1540 K (T2). This agrees well with conclusions from previous research [3,31,32] that the increasing temperature enhances the fuel-nitrogen release, mainly HCN which became the dominating nitrogen compound. Meanwhile, it can be found that the release of HCN also has its limitation as comparing the cases at 1540 K (T2) and 1630 K (T1) which have almost same release performance. This may indicate that almost all fuel-nitrogen was released into the volatile gas at these temperatures [2].

4. Conclusions

With the setup described in this paper, quantitative release history of HCN in the devolatilization stage from gasification of a biomass pellet, e.g. a straw pellet, were recorded in a spatially resolved manner. The gasification of single biomass pellets is achieved by using a specially designed laboratory-scale burner which provides controllable laminar flame environments with good repeatability and good optical access. IR-DFWM (mid-Infrared Degenerate Four-Wave Mixing) technique was adopted to probe the P(20) line of the v_1 vibrational band of HCN, which is interference-free even in combustion environments. An upconversion-based detector gave rise to increased sensitivity. The quantification of the IR-DFWM signals was achieved by an on-line calibration of the optical system with calibration gas flow containing known amounts of HCN. To account for the temperature effects, the same IR-DFWM setup was used to probe a group of hot water lines to obtain the instantaneous temperature in the interrogated volume.

The local HCN concentration in the devolatilization stage during gasification of a straw pellet was measured to be as high as 1500 ppm. We also found that the release concentration of HCN has strong dependence on the temperature of the hot flue gas environment. With the setup demonstrated in this paper, more IR-active molecules can be measured in solid fuel combustion/gasification processes. The present measurements can provide quantitative input for fuel-nitrogen modeling important in biomass utilization.

Acknowledgment

The authors appreciate financial support from the Swedish Energy Agency through CECOST, the Knut & Alice Wallenberg foundation, the Swedish Research Council (VR), the European Research Council through advanced grant TUCLA (669466), Mid-TECH (H2020-MSCA-ITN-2014, 642661) and Laserlab-Europe (H2020

EC-GA 654148). Also, we thank Mário Costa and André Moço from Instituto Superior Técnico for both fruitful discussions and providing the biomass material.

References

[1] Q. Ren, C. Zhao, *Renew. Sustain. Energy Rev.* 50 (2015) 408–418.
[2] P. Glarborg, A.D. Jensen, J.E. Johnsson, *Prog. Energy Combust. Sci.* 29 (2003) 89–113.
[3] J. Leppälahti, T. Koljonen, *Fuel Process. Technol.* 43 (1995) 1–45.
[4] W.-J. Liu, W.-W. Li, H. Jiang, H.-Q. Yu, *Chem. Rev.* 117 (2017) 6367–6398.
[5] G. Simões, D. Magalhães, M. Rabaçal, M. Costa, *Proc. Combust. Inst.* 36 (2017) 2235–2242.
[6] D.H. Rank, G. Skorinko, D.P. Eastman, T.A. Wiggins, *J. Opt. Soc. Am.* 50 (1960) 421–432.
[7] I.E. Gordon, L.S. Rothman, C. Hill, et al., *J. Quant. Spectrosc. Radiat. Transf.* 203 (2017) 3–69.
[8] S. Gersen, A.V. Mokhov, H.B. Levinsky, *Combust. Flame* 155 (2008) 267–276.
[9] N. Lamoureux, H. El Merhubi, L. Gasnot, C. Schoemaecker, P. Desgroux, *Proc. Combust. Inst.* 35 (2015) 745–752.
[10] N. Lamoureux, H. El Merhubi, X. Mercier, J.F. Pauwels, P. Desgroux, *Proc. Combust. Inst.* 34 (2013) 3557–3564.
[11] J. Kiefer, P. Ewart, *Prog. Energy Combust. Sci.* 37 (2011) 525–564.
[12] K. Richard, P. Ewart, *Appl. Phys. B* 94 (2009) 715–723.
[13] Z.S. Li, M. Rupinski, J. Zetterberg, M. Alden, *Proc. Combust. Inst.* 30 (2005) 1629–1636.
[14] Z.S. Li, M. Linvin, J. Zetterberg, J. Kiefer, M. Alden, *Proc. Combust. Inst.* 31 (2007) 817–824.
[15] Z.W. Sun, Z.S. Li, B. Li, Z.T. Alwahabi, M. Alden, *Appl Phys B – Lasers Opt.* 101 (2010) 423–432.
[16] Z.S. Li, C. Hu, J. Zetterberg, M. Linvin, M. Alden, *J. Chem. Phys.* 127 (2007) 084310.
[17] Z.S. Li, M. Rupinski, J. Zetterberg, Z.T. Alwahabi, M. Aldén, *Chem. Phys. Lett.* 407 (2005) 243–248.
[18] Z.W. Sun, Z.S. Li, A.A. Konnov, M. Aldén, *Combust. Flame* 158 (2011) 1898–1904.
[19] R.L. Abrams, R.C. Lind, *Opt. Lett.* 2 (1978) 94–96.
[20] R.L. Abrams, R.C. Lind, *Opt. Lett.* 3 (1978).
[21] G.J. Germann, R.L. Farrow, D.J. Rakestraw, *J. Opt. Soc. Am. B – Opt. Phys.* 12 (1995) 25–32.
[22] Z.W. Sun, Z.S. Li, B. Li, M. Aldén, P. Ewart, *Appl. Phys. B* 98 (2010) 593–600.
[23] Z.W. Sun, Z.S. Li, B. Li, M. Aldén, *J. Raman Spectrosc.* 42 (2011) 1828–1835.
[24] J.S. Dam, P. Tidemand-Lichtenberg, C. Pedersen, *Nat. Photonics* 6 (2012) 788.
[25] L. Høgstedt, J.S. Dam, A.-L. Sahlberg, et al., *Opt. Lett.* 39 (2014) 5321–5324.
[26] R.L. Pedersen, D. Hot, Z. Li, *Appl. Spectrosc.* 72 (2017) 793–797.
[27] W. Weng, J. Borggren, B. Li, M. Aldén, Z. Li, *Rev. Sci. Instrum.* 88 (2017) 045104.
[28] J. Borggren, W. Weng, M. Aldén, Z. Li, *Appl. Spectrosc.* 72 (2018) 946–970.
[29] R.L. Farrow, D.J. Rakestraw, T. Dreier, *J. Opt. Soc. Am. B* 9 (1992) 1770–1777.
[30] A.G. Maki, G.C. Mellau, S. Klee, M. Winnewisser, W. Quapp, *J. Mol. Spectrosc.* 202 (2000) 67–82.
[31] P. Zhou, S. Xiong, Y. Zhang, H. Jiang, Y. Chi, L. Li, *Int. J. Hydrogen Energy* 42 (2017) 18181–18188.
[32] F.-J. Tian, B.-Q. Li, Y. Chen, C.-Z. Li, *Fuel* 81 (2002) 2203–2208.